THE JOURNAL OF PHYSICAL CHEMISTRY B

Article

pubs.acs.org/JPCB

Toward Radiation-Resistant Ionic Liquids. Radiation Stability of Sulfonyl Imide Anions

Ilya A. Shkrob,*[,†] Timothy W. Marin,[†,‡] Sergey D. Chemerisov,[†] Jasmine Hatcher,[§] and James F. Wishart[§]

[†]Chemical Sciences and Engineering Division, Argonne National Laboratory, 9700 South Cass Avenue, Argonne, Illinois 60439, United States

[‡]Chemistry Department, Benedictine University, 5700 College Road, Lisle, Illinois 60532, United States

[§]Chemistry Department, Brookhaven National Laboratory, Upton, New York 11973-5000, United States

Supporting Information

ABSTRACT: Room-temperature hydrophobic ionic liquids (ILs) are considered for processing of spent nuclear fuel, including as possible replacements for molecular diluents in liquid–liquid extraction. This application requires radiation stability of the constituent ions. Previous research indicated that most of the anions that are currently used in the synthesis of ILs are prone to fragmentation under prolonged radiation exposure, which causes deterioration of the corresponding ILs. An exception to this general rule is phthalimide; unfortunately, this anion is too basic to be useful for extraction solvents, as these separations involve acidic conditions. The acidity of the imide can be increased by replacing the carbonyl groups by sulfonyl groups, which incidentally transform these imides into familiar artificial sweeteners such as saccharin. In the present study, we use electron paramagnetic resonance spectroscopy, nuclear magnetic resonance spectroscopy, and mass spectrometry to assess the radiation stability of ILs based on such "sweet" sulfonyl imide anions. Our results suggest that saccharinate and *o*-benzenedisulfonimide are remarkably stable to radiation-induced fragmentation.

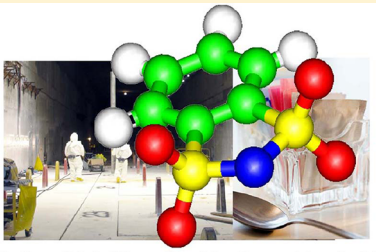

Radiation Stability of Imide-Based Ionic Liquids

1. INTRODUCTION

Room-temperature ionic liquids (ILs) continue to intrigue chemists with their unusual properties, and recent studies of these materials have resulted in an increasing number of practical applications.[1−3] One such emerging application is the use of ILs as next generation diluents for liquid–liquid metal ion extraction for advanced nuclear fuel cycles.[2−6] Since such solvents would operate in high radiation fields generated by decaying radionuclides, there is growing interest in the general radiation stability of such solvents and extraction agents (that is, metal ion complexants) in these IL solvents in particular.[5,6] It is desirable to select IL diluents that are not only resistant to radiation but also protect the extracting agents from radiolytically induced fragmentation that may result in the loss of separations efficacy and selectivity.[5−7]

When ionizing radiation interacts with matter, this interaction occurs in "spurs" (clusters of excitation/ionization events), with 10−20 eV of energy released per ionization event.[5] This energy is sufficient not only to produce highly energetic, electronically excited molecular states but also yields "hot" radical ions and prethermalized electrons.[8,9] With so much energy transferred to these molecules and ions, some of them inevitably fragment. The energy that is not expended through ionization and bond/breaking can either be released in relatively "harmless" ways (as heat, light, or reversible chemical reactions), or it can be transferred to the solute. This charge and energy transfer frequently results in chemical modifications and fragmentation of the solute. Thus, the "radioprotection" is a balancing act: a solvent that is immune to radiation damage would likely channel this damage to the solute, whose integrity may be more important than that of the solvent.[7,10,11] On the other hand, an IL diluent that rapidly disintegrates under radiation is also unacceptable.

In previous studies from our laboratory,[7−12] we examined several classes of ILs, seeking to establish the effect of composition on radiation stability. It became apparent that options to improve the radiation stability of the constituent *cations* are limited.[9] The ionization is so energetic that it occurs not only via electron detachment from the constituent anions (A^-) yielding the corresponding neutral radicals

$$A^{-**} \rightarrow e^{-\bullet} + A^{\bullet} \quad (1)$$

but also occurs in the constituent cations (C^+), resulting in the formation of radical dications

$$C^{+**} \rightarrow e^{-\bullet} + C^{2+\bullet} \quad (2)$$

that are inherently unstable due to strong Coulomb repulsion. These species quickly deprotonate, as a nearby anion can almost always serve not only as an electron donor but also as a proton acceptor.[7,9]

$$C^{2+\bullet} + A^- \rightarrow C(-H)^{\bullet} + H^{\delta+}A^{\delta-} \quad (3)$$

Received: March 5, 2012
Revised: June 29, 2012

   dx.doi.org/10.1021/jp302151c | *J. Phys. Chem. B* XXXX, XXX, XXX–XXX

For aliphatic cations (such as substituted ammonium, phosphonium, pyrrolidinium, piperidinium, and other ions), the proton transfer prevails over the electron transfer

$$C^{2+\bullet} + A^- \rightarrow C^+ + A^\bullet \quad (4)$$

and H atom loss from the aliphatic arms in reaction 3 is inevitable.[7] For aromatic cations, the fragmentation is less extensive[7,9] but still remains substantial.[9] It is not presently clear how reaction 3 or the loss of aliphatic arms in the electronically excited states of the cations could be prevented.[9]

However, such reactions do not, in fact, cause significant damage to the solvent, as the resulting C(−H)$^\bullet$ radicals are relatively unreactive and the stable reaction products have only a modest effect on the solvent properties. The same is generally correct about neutral radicals originating through electron scavenging by aromatic cations[9,12] that can be subsequently protonated at the aromatic ring

$$C^+ + e^{-\bullet} \rightarrow C^\bullet \quad (5)$$

$$C^\bullet + H^{\delta+}A^{\delta-} \rightarrow CH^{+\bullet} + A^- \quad (6)$$

A much greater problem is reaction 1, as the resulting neutral radicals A$^\bullet$ are frequently unstable.[8] Prompt fragmentation is observed for almost all anions that are currently used to synthesize ILs. Many such anions belong to the "RB$^-$ type",[8] where R is an organic group and B is an inorganic base (e.g., RCO_2^-, $ROSO_3^-$, RSO_3^-, $(RO)PO_2^-$, etc.). The corresponding neutral radicals fragment, releasing an organic radical and a neutral molecule (CO_2, SO_3, etc.).[8]

$$RB^{-**} \rightarrow e^{-\bullet} + RB^\bullet \quad (7a)$$

$$RB^\bullet \rightarrow R^\bullet + B \quad (7b)$$

This fragmentation places upper limits on the tolerable radiation exposure for the majority of common ILs as diluents for nuclear separations. While these limits do not preclude the use of most ILs in separations stages with low or moderate levels of radioactivity, we seek to identify classes of ILs that could tolerate high activity levels typical of primary processing of spent nuclear fuel.

In ref 8, we reported several exceptions to the fragmentation problem. One such exception was (pseudo)halide anions (X$^-$, such as bromide and dicyanamide, $N(CN)_2^-$), whose oxidized form stabilizes via the formation of a three-electron $X_2^{-\bullet}$ radical anion with a $\sigma^2\sigma^{*1}$ bond between the two centers. Another class of molecules excepted from fragmentation included RB$^-$ anions with unusually long-lived A$^\bullet$ radicals, such as benzoate.[9,13] It could be sufficient to extend the lifetime of such oxidized anions long enough so that they undergo back electron transfer, e.g.,

$$RB^\bullet + C^\bullet \rightarrow RB^- + C^+ \quad (8)$$

before fragmentation reaction 7b. Unfortunately, such "exceptional" RB$^-$ anions become readily protonated when the IL contacts (even weakly) acidic solutions,[14] making their corresponding ILs unsuitable for the classical extraction schemes used today in spent nuclear fuel processing, although they could be viable in newer, alkaline systems under consideration.[2] A third exceptional class involved imides, which are organic analogues of pseudohalides.

The most common representative anion of this class is bis(trifluoromethanesulfonyl)imide (also known as bistriflimide, or NTf_2^-), where Tf$^-$ denotes the CF_3SO_2 (triflyl) group.[2] In radiolysis, this anion is oxidized in reaction 1 to produce the $^\bullet NTf_2$ (imidyl) radical, which is quite stable (ref 8 and section 3.1); however, this anion still fragments through pathways involving other states generated in radiolysis. One of the fragmentation channels is dissociative electron attachment

$$NTf_2^- + e^{-\bullet} \rightarrow F^- + {}^\bullet CF_2SO_2NTf^- \quad (9)$$

which yields a $^\bullet CF_2SO_2NTf^-$ radical that can be directly observed using electron paramagnetic resonance (EPR) spectroscopy. This radiolytic generation of fluoride and hence HF is highly undesirable.[15a] Another detrimental reaction (see Figure 1S in the Supporting Information) involves the excited states of the bistriflimide anion: there are two dissociated states that involve homolytic cleavage of the C−S and O−S bonds:

$$NTf_2^{-**} \rightarrow {}^\bullet CF_3 + {}^\bullet SO_2NTf^- \quad (10a)$$

$$\rightarrow CF_3SO_2^\bullet + TfN^{-\bullet} \quad (10b)$$

The $^\bullet CF_3SO_2$ radical generated in reaction 10b is unstable,[8] dissociating to $^\bullet CF_3$ and SO_2;[16,17] thus, both of these channels result in the elimination of the trifluoromethyl group.[16] This small, diffusive, and reactive radical recombines with other radicals generated in the IL,[8,9,15b,16] and the release of SO_2 results in the production of sulfites and sulfates;[17] these reactions are detrimental to performance of the ILs. Thus, it is not sufficient to inhibit reaction 7b, as the anion also needs to be resistant to fragmentation following electronic excitation and/or dissociative electron attachment (exemplified in reactions 9 and 10 for NTf_2^-).

A common approach to improving such stability involves introducing aromatic groups that can spread the excess charge or excitation through their π-orbitals, avoiding the localization of electron density on a few atoms, which favors fragmentation. In this regard, the most important result of ref 8 was our observation that an aromatic imide anion, phthalimide (anion **a** in Scheme 1) was resistant to fragmentation. Following the

Scheme 1. The Anions of (a) Phthalimide, (b) Saccharinate, (c) *o*-Benzenedisulfonimide, and (d) Acesulfamate

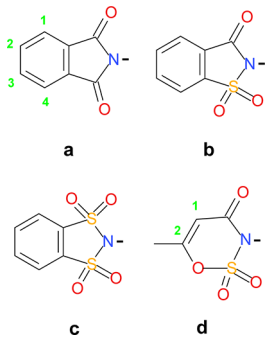

notations introduced in Scheme 2, the oxidation and reduction of the imide anion (>N$^-$) results in the following reactions:

$$>N^{-**} \rightarrow >N^\bullet + e^{-\bullet} \quad (11)$$

$$>N^- + e^{-\bullet} \rightarrow >N^{2-\bullet} \quad (12)$$

The latter dianion is a strong base that is immediately protonated to yield an imide radical anion >NH$^{-\bullet}$ (structure **1a** in Scheme 2, where **a** stands for the anion as specified in Scheme 1)[8]

$$>N^{2-\bullet} + >N^{\delta-}H^{\delta+} \rightarrow >NH^{-\bullet} + >N^- \quad (13)$$

dx.doi.org/10.1021/jp302151c | J. Phys. Chem. B XXXX, XXX, XXX−XXX

Scheme 2. The Main Types of Radicals Derived from Aromatic Imide Anions: (1) Protonated Electron Adduct, >NH$^{-\bullet}$ Radical; (2) Oxidized Anion, >N$^{\bullet}$; (3) One of the Four Possible H Atom Ring-Adducts; (4) N−N $\sigma\sigma$ Bound Dimer Radical Anion, {>N−N<}$^{-\bullet}$; (5) Ring-Opening *o*-Substituted Phenyl Radical Derived from Radical 2; (6) Ketyl Radical Resulting from H Atom Addition to a Carbonyl Bond of the Parent Anion; (7) Contracted Cyclic Imidyl Radical 2 Resulting from the Elimination of a Group[a]

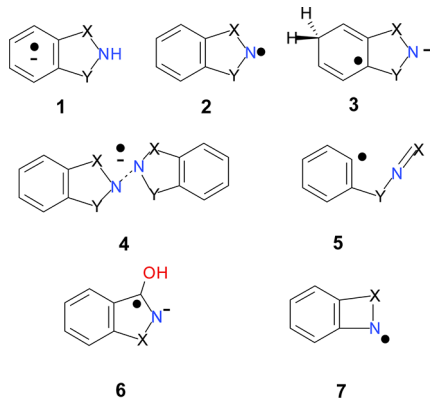

[a]Symbols X and Y stand for carbonyl or sulfonyl group(s). Throughout the text, reference to radicals a−d associated with each of the structures below (e.g., 1a, 3b, 7c) is tied to anions a−d shown in Scheme 1.

Imidyl radical **2** (the product of reaction 11) is very reactive even at cryogenic temperatures, as many other N-centered radicals of this type, and it can readily abstract an H atom from the aliphatic arms of the cations

$$>N^{\bullet} + C^{+} \rightarrow >N^{\delta-}H^{\delta+} + C(-H)^{\bullet} \quad (14)$$

For this reason, observation of radical **2** in the IL is generally unlikely, but this radical can be observed in the corresponding alkali salts. Both radicals **1a** and **2a** were observed in radiolysis of phthalimide salts at low temperature.[8] Figure 2S in the Supporting Information shows the energy diagram for this anion: the only dissociative channel for the corresponding imidyl radical (structure **2a** in Scheme 2) is the scission of the C_r-C_O bond, where the subscripts denote the ring (r) and carbonyl (O) carbons, respectively (structure **5** in Scheme 2). This isomerization is known to occur for cyclical imides,[18] but it was not observed for phthalimide in ILs,[8] as the corresponding reaction is endergonic by ∼0.4 eV (see Table 1). Another possible fragmentation channel, decarbonylation, is also endergonic by ∼1.1 eV. Further stabilization of the oxidized anion could occur through the formation of a two-center, three-electron bond between the nitrogens of the imidyl radical and the parent imide anion

$$>N^{-} + >N^{\bullet} \rightleftharpoons \{>N-N<\}^{-\bullet} \quad (15)$$

that yields a C_2 symmetrical dimer radical anion **4** in Scheme 2. Figure 3S(a) in the Supporting Information exhibits the structure of this dimer anion. This species is known to occur by one-electron reduction of diphthalimide.[19] Our calculations suggest that the stabilization energy of reaction 15 is ∼0.8 eV (see Table 1).

Reaction 15 is somewhat analogous to the formation of dimer radical cations for aromatic molecules in molecular solvents that serve to make them more efficient traps for positive charge in such solvents.[20] This N−N interaction could be weakened in the presence of cations, as the monomer anion is more strongly solvated than the dimer anion.[12] However, even if reaction 15 is shifted to the left side, it can still fleetingly stabilize the excited imidyl radical **2** generated in reaction 11, thereby protecting this radical from fragmentation. The excited phthalimide anion is also less likely to fragment, as the excitation is localized mainly on the benzene ring and the diradical generated via bond scission is likely to recombine (whereas for NTf_2^- the two fragments can escape recombination). Indeed, in acetonitrile solution, the photoexcited phthalimide anion is known to react by charge transfer

$$>N^{-}*(S_1) + >N^{\delta-}H^{\delta+} \rightarrow >N^{\bullet} + >NH^{-\bullet} \quad (16)$$

yielding radicals **1a** and **2a** in Scheme 2.[21] Typical reactions[22,23] of these radicals involve H abstraction by the imidyl radical **2a** from an H atom donor (analogous to reaction 14) followed by radical addition of the resulting radical to the C_O carbon in radical **1a**, as shown in Scheme 1S in the Supporting Information. These reactions do not fragment the anion.

Table 1. Gas-Phase Electronic Energies for Aromatic Imides (Labeled as in Schemes 1 and 2) (the footnotes below are related to electronic energy contribution only)

energy (eV)	a	b	c	d
PA[a] of >N$^-$ anion	15.1	14.3	13.7	14.14
EA[b] of >NH imide	1.12	1.08	1.01	2.03
ADE[c] of >N$^-$ anion	3.98	4.24	4.33	4.42
triplet energy for >N$^-$ anion	2.88	2.77	3.12	
BDE[d] for C_1-C bond in radical **2**	0.39	0.93		1.40
BDE[d] for N−X bond in radical **2**		2.68[e]	3.37[f]	
BDE[d] for N−X bond in >N$^-$ triplet		1.49[e]	0.20[f]	
BDE[d] (H−C in radical **3**)	1.32[g]	1.35[h]	1.41[g]	1.74[i]
BDE[d] (H−N in radical **1**)	2.58	1.75	1.08	
elimination of CO from radical **2**	−1.14[j]	−2.87		0.52
elimination of SO_2 from radical **2**		0.21	−1.24	0.36
BDE[d] for radical **4**[k]	0.79	0.43	0.35	

[a]Proton affinity. [b]Electron affinity. [c]Adiabatic electron detachment energy. [d]Bond dissociation energy. [e]X=C. [f]X=S. [g]2,2′-adduct. [h]4,4′-adduct. [i]1,1′-adduct. [j]With the formation of radical **5**. [k]C_2 symmetry.

These properties are offset by a crucial shortcoming: phthalimide is a strong base (pK_a 8.3 in aqueous solution), so it cannot be used in IL diluents operating in acidic solutions. Can the structural motif be retained but the pK_a be decreased? It is known[24,25] that replacement of the carbonyl groups by sulfonyl groups increases the acidity of imides. Scheme 1 shows three phthalimide-inspired anions: saccharinate (**b**, pK_a 1.48), *o*-benzenedisulfonimide (**c**, pK_a −4.1), and acesulfamate (**d**, pK_a ≈ 2.0). Interestingly, all of these anions are well-known artificial sweeteners.

Below, we demonstrate that saccharinate and *o*-benzenedisulfonimide are resilient to radiation damage, while acesulfamate is less stable. ILs based on the saccharinate and acesulfamate anions have been studied as "greener" solvents,[26−28] since both of these anions are relatively nontoxic and environmentally benign. The latter propensity stems from the fact that no known living organism metabolizes such imides, which is a consequence of their exceptional resilience to redox fragmentation. Where Mother Nature fails, so does ionizing radiation.

We emphasize that our conclusions have preliminary, qualitative character, as we focused on direct observation of

dx.doi.org/10.1021/jp302151c | J. Phys. Chem. B XXXX, XXX, XXX−XXX

fragment *radicals* (sections 3.1−4); if there are diamagnetic fragment products generated in redox and excited-state reactions of the imide anions, such products would evade EPR detection. Nevertheless, the resilience of the aromatic imide anions is also attested by product analyses given in section 3.5. Put together, these results are strongly suggestive that this class of ionic liquids indeed has exceptional radiation stability, which makes such substances appealing choices for practical applications involving decaying radionuclides.

To conserve space, some sections, schemes, tables, and figures have been placed in the Supporting Information. Such figures have designator "S" (e.g., Figure 1S). Since EPR spectra of irradiated frozen ILs are complicated, as radicals generated both from the anions and cations contribute to the EPR spectrum, we preempt the discussion of these EPR spectra by examining alkali salts of the imides. Despite this structural "simplicity", the resulting EPR spectra are still rather complex, as both electron centers (such as radical **1**) and hole centers (such as radicals **2**) contribute to these spectra. Furthermore, since organic cations in ILs serve as acceptors of electronic excitation, some fragmentation reactions that are observed in the alkali salts are not observed in the IL matrixes.

2. EXPERIMENTAL AND COMPUTATIONAL METHODS

Synthetic, spectroscopic, and computational approaches used in this study were similar to those used in prior work.[8,9] All of the reagents were obtained from Aldrich except for the chemicals whose synthesis is given in section 1S of the Supporting Information. The corresponding ^{1}H and ^{13}C NMR spectra are given in Figures 4S−7S and the mass peaks are summarized in Table 1S and Figure 8S(a) (Supporting Information). Crystallographic parameters for potassium *o*-benzenedisulfonimide monohydrate are given in section 2S (Supporting Information, see Figure 8S(b) for the crystal structure).

Samples were frozen by rapid immersion in liquid nitrogen and irradiated to 3 kGy at 77 K using 3 MeV electrons (1 Gy = 1 J/kg of the absorbed energy). The radicals were observed using a 9.44 GHz Bruker ESP300E spectrometer, with the sample placed in a flow He cryostat (Oxford Instruments CF935). The magnetic field $\boldsymbol{B}$ and the hyperfine coupling constants (hfcc's) are given in the units of Gauss (1 G = 10^{-4} T). If not stated otherwise, the first-derivative EPR spectra were obtained at 50 K using 2 G modulation at 100 kHz. The radiation-induced EPR signal from the E_{γ}' center in the Suprasil sample tubes is not shown in the EPR spectra.

The calculations of the hfcc's and the structures for the radicals were carried out using a density functional theory (DFT) method with the B3LYP functional[29] and 6-31+G(d,p) basis set from Gaussian 98.[30] In the following, a_{iso} denotes the isotropic hfcc corresponding to the hfc tensor $\boldsymbol{A}$. Powder EPR spectra were simulated using first-order perturbation theory. For convenience, the principal values of the *g*-tensor in Table 2 and elsewhere are reported as $\delta g_{\nu\nu} = (g_{\nu\nu} - 2{\cdot}\mathbf{1}) \times 10^4$, where $\nu = x, y, z$ are the principal axes.

Product analyses of irradiated samples were carried out using nuclear magnetic resonance (NMR) and mass spectrometry. Nitrogen-purged ionic liquids (1.5 mL) were placed in sealed water-cooled borosilicate tubes and irradiated by 3 MeV electrons to a total dose of 2.45 MGy using a dose rate of 6.8 kGy/s. We stress that the samples for product analysis were irradiated to a much higher dose and temperature than the samples for EPR studies. During the irradiation, the sample temperature increased to 40 °C due to heat deposition in the sample. ^{1}H, ^{14}N, and ^{13}C NMR spectra were obtained in dimethylsulfoxide-d_6 (DMSO-d_6), using an Avance DMX 500 MHz spectrometer (Bruker); the chemical shifts are given vs tetramethylsilane (TMS). Tandem electrospray ionization mass spectra (ESI MS_n) were obtained using a Thermo Scientific LCQ Fleet ion trap mass spectrometer operating either in positive or negative modes ($MS_n^{\pm}$) using a spray voltage of 4.4 kV. MS_1 corresponds to the first quadrupole, and MS_2 corresponds to collision induced dissociation (of mass selected ions) modes of operation. Liquid samples were injected in dilute acetonitrile solutions.

Table 2. *g*-Tensors ($\delta g = (g - 2{\cdot}1) \times 10^4$) and Hyperfine Coupling Tensors *A* for ^{1}H and ^{14}N Nuclei Obtained from Simulation of EPR Spectra for Radicals Observed at 50 K

radical	cation	(δg_{xx}, δg_{yy}, δg_{zz})	(A_{xx}, A_{yy}, A_{zz}) (G)	a_{iso} (G)
1b[a]	K^+	34.5[b]	$^{1}H_3$ (−10.4, −6.5, −3)	−6.1
1c[c]	K^+	(51, 39, 23)	$^{1}H_{2,3}$ (0, −3.8, −5.4))	−3.3
1c[c]	$P_{666,14}^+$	(43, 38, 19)	$^{1}H_{2,3}$ (0, −5.1, −5.6))	−3.6
$^{\bullet}NTf_2$[d]	Li^+	41 (xx)	^{14}N: (38.3, ∼0, ∼0)	12.8
		43 (xx)	^{14}N: (40.7, ∼0, ∼0)[e]	13.6[e]
$^{\bullet}NTf_2$[f]	EtPy-d_{10}^+	39 (xx)	^{14}N: (35, ∼0, ∼0)	11.7
			^{14}N: (31.5, ∼0, ∼0)	10.5
2a[d]	Na^+	37 (xx)	^{14}N: (44, ∼0, ∼0)	14.7
2b[g]	K^+	(53, 95, 0)	^{14}N: (34, ∼0, ∼0)	11.3
2c[d]	K^+	41 (xx)	^{14}N: (33.1, ∼0, ∼0)[h]	11.0
7d[i]	K^+	(40, 40, 30)	$^{1}H_{Me}$	12.1[b]
			$^{1}H_1$	−5.0[b]
			^{14}N(19.5, 0, 0)	6.5
8[j]	K^+	(60, 60, 80)	^{1}HN	5.5[b]
			H^{14}N	3.0[b]
9[k]	K^+	(40, 40, 0)	$^{1}H_{Me}$	19.6[b]
			$^{1}H_{1a}$	52
			$^{1}H_{1b}$	∼0
10[l]	K^+	37[b]	$^{1}H_a$ (−21.5, −14.7, −6.1)[m]	−14.2
			$^{1}H_b$ (−23.5, −15, −6.5)[m]	−15.0
			$^{1}H_c$ (−19.6, −14.1, −6.4)[m]	−13.3
10[n]	K^+	38[b]	$^{1}H_{a,b}$ (−22, −7.5, −7.0)	−14.5
			$^{1}H_c$ (−20.4, −13.2, −6.0)	−13.2

[a]See Figure 3. [b]Anisotropy neglected. [c]See Figure 8. [d]See Figure 1a. [e]At 130 K. [f]See Figure 1b, two variants of the spin center. [g]See Figure 2. [h]Majority variant. [i]See Figure 17S in the Supporting Information (optimum set 2). [j]See Figure 11. [k]See Figure 16S in the Supporting Information (optimum set 1). [l]At 100 K, see Figure 13. [m]From B3LYP/6-31+G(d,p) calculation. [n]At 200 K, see Figure 18S in the Supporting Information.

3. RESULTS

3.1. Imidyl Radicals. Before considering each of the anions in Scheme 1 separately, we examine a feature common to all imide radiolysis, that is, the formation of radical **2** in reaction 11. To this end, we examined a series of alkali salts of aromatic imides, as the resulting imidyl radicals are more stable in these salts at low temperature, as the abstraction of aromatic hydrogens is less facile than reaction 14 involving aliphatic C−H bonds.

It is known from the literature (see Table 3S in the Supporting Information for a compilation of the reported and calculated spin parameters) that aminyl and imidyl radicals have

dx.doi.org/10.1021/jp302151c | J. Phys. Chem. B XXXX, XXX, XXX−XXX

a hfcc tensor for the ^{14}N nucleus in which $A_{xx} \approx 30-50$ G and $A_{yy} \approx A_{zz} \approx 0$. The resulting EPR spectra exhibit two well-separated outer lines corresponding to the external magnetic field B of the spectrometer aligned with axis x of this hfcc tensor (which is perpendicular to the >N$^{\bullet}$ plane). Our DFT calculations suggest that radicals **2a–d** (Scheme 2) also have $|A_{yy,zz}| < 1$ G and $A_{xx} \approx 33-35$ G, which favorably compares to $A_{xx} \approx 31$ G reported for the succinimidyl radical (Table 3S and Figure 9S(a), Supporting Information). As suggested by simulations shown in Figure 9S(b) (Supporting Information), contracted imidyl radicals **7b** and **7c** (Scheme 2) that are obtained from their parent radicals **2b** and **2c** by a loss of the sulfonyl group would have rather different EPR spectra due to the strong coupling (~6–8 G) of the unpaired electron density to $H_{2,4}$ carbons in the benzene ring. Our DFT calculations indicate that such an elimination is one of the possible pathways for fragmentation of radical **2** (see section 4).

Figure 1a exhibits EPR spectra obtained in the radiolysis of polycrystalline lithium bistriflimide, sodium phthalimide, potassium saccharinate, and potassium *o*-benzenedisulfonimide at 77 K. In these EPR spectra, one can clearly observe the outer $M_I(^{14}N) = \pm 1$ lines of radicals **2** that correspond to the $B||x$ resonances. Table 2 gives the summary of the δg_{xx} and $A_{xx}[^{14}N]$ parameters for these imidyl radicals. To observe these resonance lines in frozen ILs without interference from other radicals, we synthesized perdeuterated *N*-ethylpyridinium bistriflimide (Figure 1b). As the deuteron (spin-1 nucleus) has a smaller magnetic moment than the proton (spin-1/2 nucleus), the hfcc's for the former nuclei are only 15.3% of the latter, which causes the "collapse" of the resonance lines from the cation-derived radicals to an unresolved feature at the center of EPR spectrum. The $M_I(^{14}N) = \pm 1$ lines ($B||x$) from two variants of the imidyl radical are clearly observed in this solid matrix (Figure 1b), in the same field as these lines appear in irradiated Li NTf_2. Since hfcc's on the ring protons are negligibly small in all of these imidyl radicals (Table 2S, Supporting Information), these protons can be neglected in EPR simulations.

In Figure 2, we simulated the EPR spectrum of radical **2b** observed in irradiated potassium saccharinate assuming coaxial

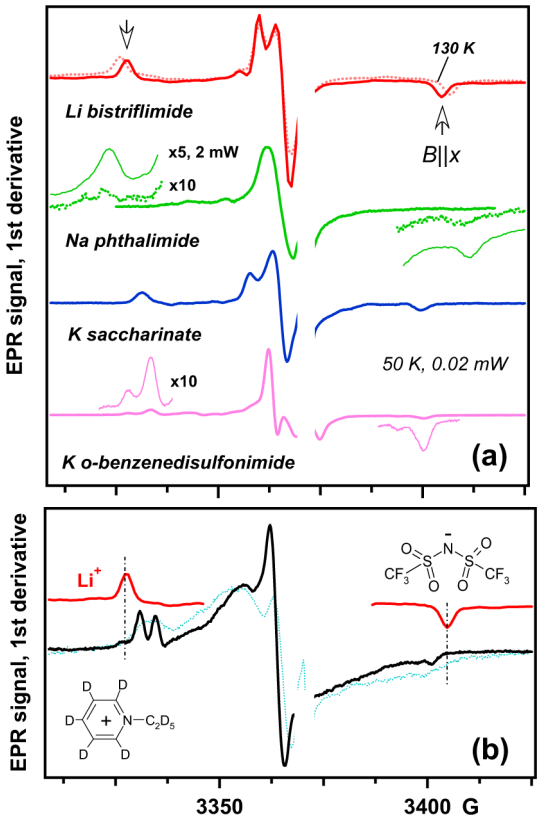

Figure 1. (a) First-derivative EPR spectra (50 K, 0.02 mW) of irradiated alkali imides (from top to bottom: lithium bistriflimide, sodium phthalimide, and potassium saccharinate). For the upper trace, the dashed line corresponds to the EPR spectrum of the irradiated sample warmed to 130 K. All of these EPR spectra exhibit the $B||x$ components (indicated by arrows) corresponding to $M_I(^{14}N) = \pm 1$ resonance lines of imidyl radical **2** in Scheme 2. (b) The comparison of EPR spectra from irradiated frozen lithium and *N*-ethylpyridinium-d_{10} (EtPy-d_{10}) bistriflimides. The resonance lines of the imidyl radicals are indicated by vertical dash-dot lines. The resonance line from the E'_γ center in the irradiated sample tube has been deleted from the experimental EPR spectra.

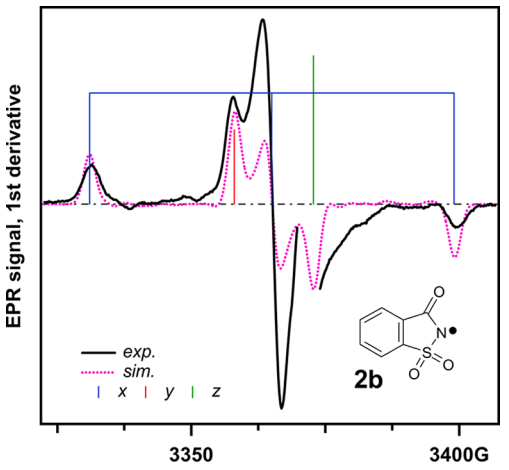

Figure 2. Simulation of the EPR patterns observed in irradiated potassium salts of saccharinate from Figure 1. The experimental traces are given by solid lines; simulated EPR spectra for radical **2b** are shown by dotted lines. The fit parameters are given in Table 2. The centroids of resonance lines are indicated with vertical lines (see the inset).

g and $A(^{14}N)$ tensors (see Table 2 for simulation parameters), corresponding to an isotropic hfcc constant of $a(^{14}N) \approx 11.3$ G (vs calculated $a = 10.9$ G, see Table 3S, Supporting Information). The narrow resonance line overlapping with the $M_I(^{14}N) = 0$ line of radical **2b** is from radical **1b** (section 3.2). The calculated isotropic g-factor, $g_{iso} \sim 2.0052$, favorably compares with the typical g-factors observed for amidyl and imidyl radicals (2.0030–2.0075). Note that the $B||z$ component overlaps with the E'_γ line from the sample tube.

Closer examination of the EPR spectrum from irradiated sodium phthalimide reveals a narrow singlet that overlaps with the resonance lines of radical **2a**. The same resonance line is observed in ILs consisting of phthalimide.[8] In ref 8, we demonstrated that this singlet line belongs to radical **1a** (see EPR simulations in Figure 9S(a), Supporting Information). For potassium saccharinate (Figure 10S, Supporting Information) and potassium *o*-benzenedisulfonimide (Figure 11S, Supporting Information) in addition to the resonance lines from radicals **1b** and **1c**, respectively, there is also a low-yield radical that persists to 150–300 K when both radicals **1** and **2** decay. This radical can also be observed at low temperature using high microwave

dx.doi.org/10.1021/jp302151c | J. Phys. Chem. B XXXX, XXX, XXX–XXX

power, as it is less saturable than radicals **1** and **2** (Figure 11S(a), Supporting Information). This persistent radical does not exhibit hyperfine structure; in potassium *o*-benzenedisulfonimide, it corresponds to a spin center with δg = (170, 70, 24) (Figure 11S(b), Supporting Information). Subtracting this feature from the EPR spectrum obtained at 50 K removes the interfering signal, and the EPR spectra shown in Figure 1a have been corrected in this way.

3.2. Saccharinate. Figures 3 and 4 exhibit EPR spectra obtained from irradiated trihexyltetradecyl phosphonium

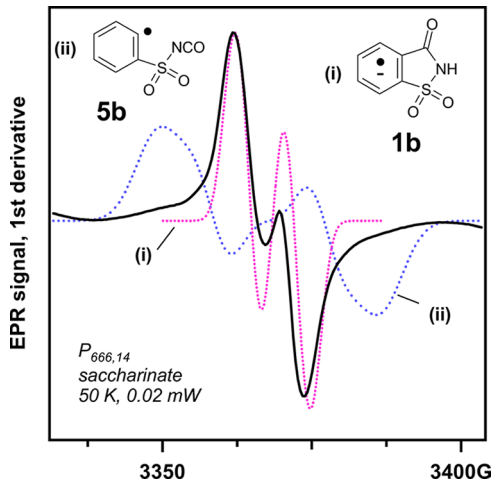

Figure 3. The EPR spectra from irradiated $P_{666,14}$ saccharinate obtained at 50 K (the microwave power is given in the plot). Simulated EPR spectra for the corresponding (i) radical **1b** (see Table 2 for fit parameters) and (ii) radical **5b** (Table 2S, Supporting Information) are superimposed on the plot.

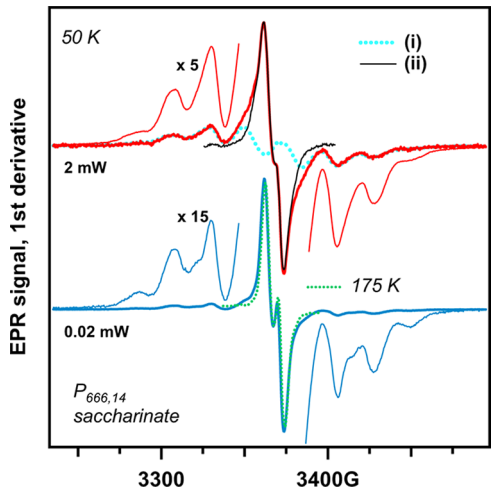

Figure 4. Wide-sweep EPR spectra for the system shown in Figure 3. The narrow-line EPR signal from radical **1b** saturates at lower microwave power than the underlying C(−H)• radicals. Superimposed on this trace are (i) the EPR spectra from irradiated $P_{666,14}$ chloride (dashed line), which arises mainly from the C(−H)• radicals, and (ii) the difference trace that is mainly from radical **1b**. In the lower trace, the normalized EPR spectrum from $P_{666,14}$ saccharinate obtained at 175 K is superimposed on the 50 K trace. At this elevated temperature, most of the C(−H)• radicals decay (cf. Figure 6).

($P_{666,14}$) saccharinate. The narrow, easily saturable doublet with g_{iso} = 2.0035 in Figure 3 is from radical **1b** (see simulated trace in the same plot and Table 2), which (unlike radical **1a**, see Figure 9S(a) and Table 2S, Supporting Information) has a non-negligible hfcc on the H_3 proton with $a_{iso}[^1H] \sim -3.5$ G in the ring. C_r-S or C_r-C_O bond dissociation (via the loss of CO or SO_2 or by scission) produces an *o*-substituted phenyl radical **5b** (structure ii in Figure 3) that would yield the EPR spectrum indicated by trace ii. It is seen that such phenyl radicals are not generated in the radiolysis of this IL.

Figure 4 shows EPR spectra obtained over a wider field range. In the wings, there are groups of resonance lines from C(−H)• radicals in the aliphatic arms of the phosphonium cation.[7] These radicals are generated via reactions 3 and 14. In the upper trace, the normalized EPR spectrum of irradiated $P_{666,14}$ chloride (trace i) is superimposed on the EPR spectrum of irradiated $P_{666,14}$ saccharinate. In the former trace, the entire EPR signal is from the C(−H)• radicals; their EPR signal can be subtracted to reveal the spectrum of radical **1b** without interference. Alternatively, the sample can be warmed to 175 K (lower trace); at this temperature, radical **1b** still persists, while the C(−H)• radicals decay (Figure 4). Both methods demonstrate that radical **1b** is the major anion-related radiolysis product; double integration of EPR spectra obtained at low microwave power indicates near parity in the yield of the alkyl radicals (the products of cation oxidation) and radical **1b** (the product of anion reduction), as could be expected on chemical grounds.

Figures 5 and 6 exhibit the evolution of the EPR spectra with increasing temperature. While the doublet from radical **1b**

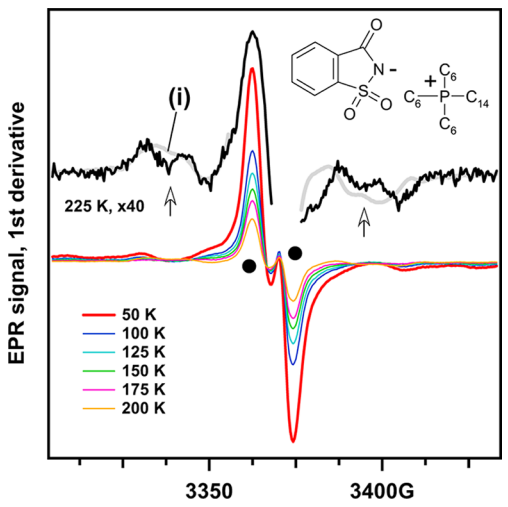

Figure 5. Temperature evolution of the EPR spectra for the same system as in Figure 3. As the sample warms, the doublet of radical **1b** (filled circles) becomes weaker, but this radical persists to 200 K. Above 210 K, this radical decays and a much weaker underlying signal from a cation-derived secondary radical becomes visible (at the top, indicated by arrows). The same secondary radical (trace i) was also observed in irradiated $P_{666,14}$ phthalimide.

systematically decreases in amplitude, its appearance does not change with temperature (Figure 5), whereas the alkyl radicals (whose resonance lines are indicated by open circles in Figure 6) gradually decay. Above 170 K, a "split" doublet of lines appears from a radical that we tentatively attribute to *cis*-$R_3P^+C^\bullet CHR'$, which is indicated with arrows in Figures 5 and 6. These features are also observed in $P_{666,14}$ phthalimide (trace i in Figure 5) and some other compounds of this cation,[7,8] and so these features belong to a radical derived from the *cation*; as our focus is on the anion chemistry, the identity of this radical

dx.doi.org/10.1021/jp302151c | J. Phys. Chem. B XXXX, XXX, XXX−XXX

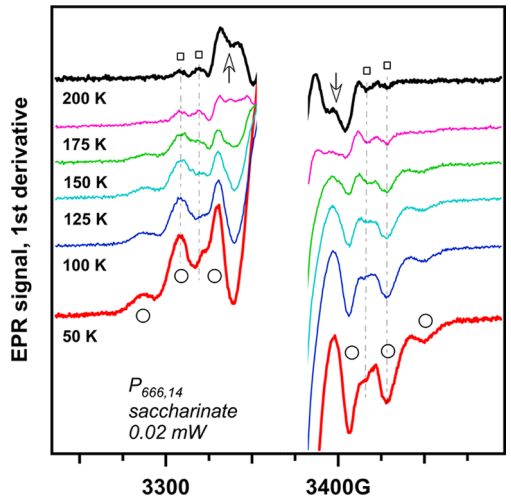

Figure 6. The wings of EPR spectra shown in Figure 5. This plot illustrates the gradual disappearance of the features from the C(−H)• radicals (open circles) and the onset of the features indicated with arrows in Figure 5. Open squares and vertical lines indicate the positions of resonance lines from radical **3b**.

is not discussed further. A closer examination of the 200 K trace reveals weak resonance lines whose positions coincide with the positions of such lines in irradiated potassium saccharinate (Figure 12S, Supporting Information). For phthalimide, similar resonance lines were observed, and we attribute these lines to radical **3a**.[8] The likely pathway to this radical is the release of an H atom from radiolytically generated acids (formed in reactions 3 and 14) or electronically excited cations

$$>N^{\delta-}H^{\delta+} + e^{-\bullet} \rightarrow >N^{-} + H^{\bullet} \quad (17)$$

$$C^{+}** \rightarrow C(-H)^{+\bullet} + H^{\bullet} \quad (18)$$

followed by addition of these H atoms to the benzene ring

$$>N^{-} + H^{\bullet} \rightarrow \text{radical } \mathbf{3} \quad (19)$$

Note that radical **3** is an isomer of radical **1**.

In Figure 12S of the Supporting Information, we juxtaposed the EPR spectra with the simulated EPR spectra for these adducts obtained using the calculated hfcc parameters given in Table 2S (Supporting Information). This comparison indicates that the H atom adds mainly to positions 2 and 3 in the benzene ring (Scheme 1); the same two positions were also attacked in phthalimide, suggesting similarity of the reaction mechanism. The only features indicating fragmentation of the anion were the resonance lines of the formyl radical (Figure 13S, Supporting Information) that were observed in the radiolysis of potassium saccharinate. No such features were observed for $P_{666,14}$ saccharinate.

3.3. *o*-Benzenedisulfonimide. Figure 11S (Supporting Information) shows EPR spectra for irradiated potassium *o*-benzenedisulfonimide. Some features of this EPR spectrum are similar to the EPR spectrum for potassium saccharinate (see Figure 1a), but the features at the center (where resonance lines from radicals **1** and **2** overlap) are different. As suggested by simulations shown in Figure 9S(a) (Supporting Information) using calculated parameters given in Table 2S (Supporting Information), the corresponding imidyl radicals **2b** and **2c** have similar spectra (except for the degree of anisotropy in their ***g***-tensors), whereas EPR spectra of corresponding radicals **1b** and **1c** would be quite different, since the unpaired electron in these radical anions is coupled to either one (H_3) or two ($H_{2,3}$) protons in the benzene ring, respectively. Since the interfering signal from the imidyl radical is absent in these ILs, we first examine EPR spectra from $P_{666,14}$ *o*-benzenedisulfonimide shown in Figure 7.

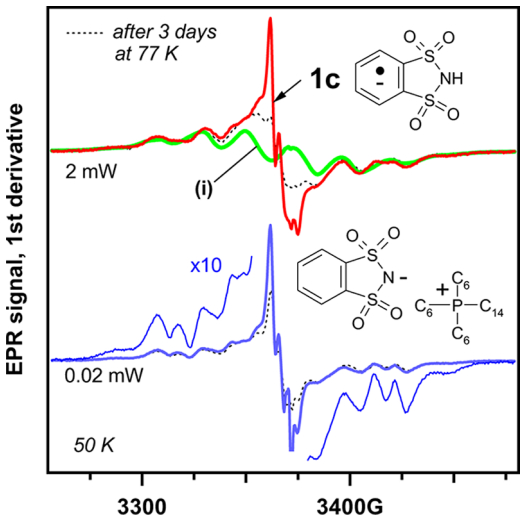

Figure 7. Like Figure 4 for $P_{666,14}$ *o*-benzenedisulfonimide at 50 K. Trace i is the EPR spectrum from $P_{666,14}$ chloride. The solid line traces were obtained immediately after radiolysis of the sample at 77 K, and the dashed traces were obtained after 3 days of storage in liquid nitrogen. The decaying EPR signal is from radical **1c**.

This EPR spectrum (like that shown for the $P_{666,14}$ saccharinate in Figure 3) consists of a set of narrow resonance lines of radical **1c** superimposed on the resonance lines from the C(−H)• radical. When this irradiated sample was stored for 3 days at 77 K, this set of lines slowly decayed, and subtraction of the EPR spectra before and after this isothermal annealing yielded (mainly) the spectrum of radical **1c** shown in Figure 8,

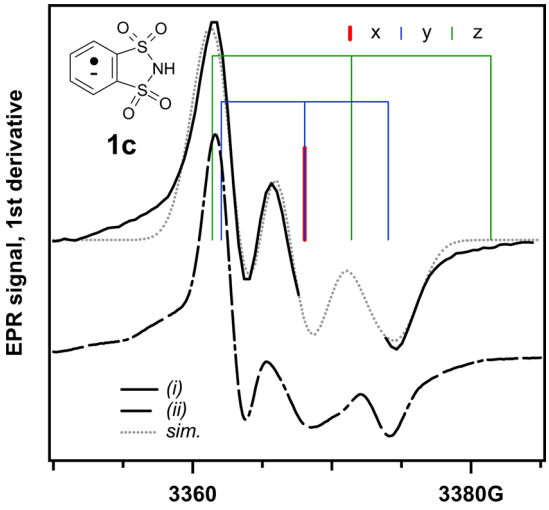

Figure 8. Trace i is the difference trace from Figure 7 (before and after isothermal annealing at 77 K) obtained at low microwave power (0.02 mW) to avoid saturation and fit using the simulation parameters for radical **1c** given in Table 2. The centroids are indicated in the plot with vertical lines. Trace ii is the central part of the EPR spectrum from irradiated potassium *o*-benzenedisulfonimide at 50 K obtained at 2 mW.

dx.doi.org/10.1021/jp302151c | J. Phys. Chem. B XXXX, XXX, XXX−XXX

trace i. Simulation of the EPR spectrum shown therein (see Table 2 for optimized spin parameters) yielded $a(^1H_{2,3}) \approx -3.6$ G (vs estimated −5.8 G in Table 2S, Supporting Information). Almost exactly the same EPR spectrum is observed for irradiated potassium *o*-benzenedisulfonimide (trace ii in Figure 8 and Table 2) after the correction for the interference from the persistent radical (Figure 11S(b), Supporting Information). We conclude that in both systems the same radical species is generated, and the elucidated spin parameters are consistent with those expected for radical **1c** (from our DFT calculations).

In addition to this radical, another anion-derived radical is observed (Figures 9 and 14S, Supporting Information) whose

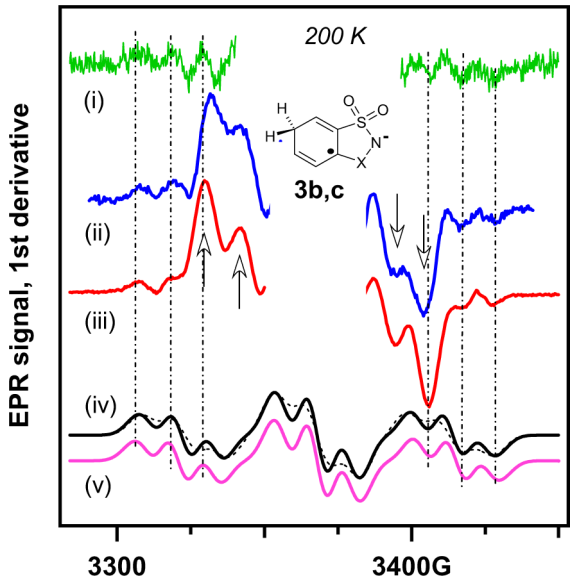

Figure 9. A comparison of the EPR spectra from (i) potassium saccharinate, (ii) $P_{666,14}$ saccharinate, and (iii) $P_{666,14}$ *o*-benzenedisulfonimide irradiated at 77 K and observed at 200 K. The vertical lines indicate the lines of radicals **3**, and the arrows indicate the resonance lines of a cation-related radical in Figures 5 and 6. Traces iv and v are EPR spectra simulated using the spin parameters calculated for radicals **3b** (2,2′, solid line; 3,3′, dashed line) and **3c** (2,2′) reported in Table 2S, Supporting Information.

resonance lines persist to 215 K when both radicals **1c** and C(−H)• decay (Figure 14S(a) and 14S(b), Supporting Information). The resonance lines of these radicals are already seen at 50 K, but these lines overlap with the resonance lines of the C(−H)• radicals. In Figure 9, we compare the EPR spectra obtained at 200 K for potassium saccharinate, $P_{666,14}$ saccharinate, and $P_{666,14}$ *o*-benzenedisulfonimide. The same resonance lines are observed in all three systems, and a comparison of these EPR spectra to simulated EPR spectra of radicals **3** is shown in Figure 9 (2,2′ and 3,3′ isomers) using the computed spin parameters given in Table 2S (Supporting Information). These comparisons indicate that the observed features are from the H-adduct radicals **3** generated in reaction 19, which are structural isomers of radicals **1**. As was the case for saccharinate, no radical **2c** was observed in this ionic liquid, suggesting that it promptly decays via reaction 14.

3.4. Acesulfamate. EPR spectra observed for irradiated potassium acesulfamate were complex (Figure 10), and these spectra exhibited significant evolution when the sample was warmed to 200 K (Figure 15S, Supporting Information). This indicates the presence of several radicals. The predominant

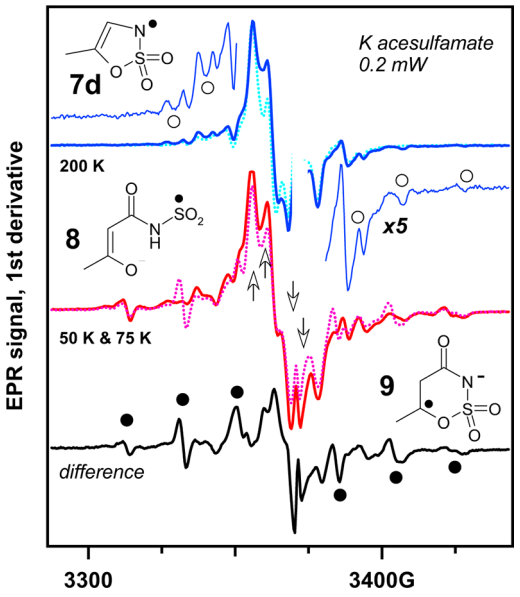

Figure 10. The EPR spectra of irradiated potassium acesulfamate. In the middle tier are the spectra obtained at 50 K (solid line) and 75 K (dashed line) with the resonance lines from radical **8** (cf. Figure 11) indicated with arrows. At the top is the EPR spectrum observed at 200 K (solid line, with the portion of this spectrum magnified) and 50 K (after a cool down, dashed line). Empty circles indicate groups of resonance lines attributed to radical **7d**. The difference of the 50 and 200 K traces is shown at the bottom; this EPR spectrum reveals the resonance lines attributed to radical **9** (filled circles). See Figures 16S and 17S in the Supporting Information for simulations of these EPR spectra and Table 2 for fit parameters.

feature in these EPR spectra is indicated by arrows in Figure 10 and also plotted separately in Figure 11. In section 4, we identify these resonance lines with fragment radical ion **8** shown in the inset in Figure 11 (see Table 2 for spin parameters). This radical anion can be thought of as radical **1d** that fragmented at the S−O bond. Radical **8** is quite stable, and it persists to 200 K. Superimposed onto the EPR spectrum of

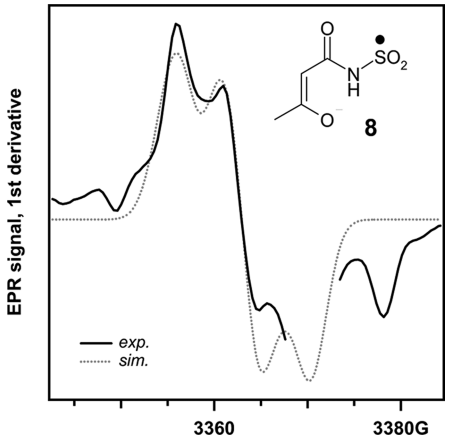

Figure 11. Simulated EPR spectrum of irradiated potassium acesulfamate from Figure 10 (50 K trace). The suggested structure for the progenitor of this EPR spectrum (radical **8**) is shown in the inset (see Table 2 for spin parameters and Scheme 2S in the Supporting Information for energetics of fragmentation). The resonance line from the E'_γ center in the irradiated sample tube has been deleted from the experimental EPR spectra.

dx.doi.org/10.1021/jp302151c | J. Phys. Chem. B XXXX, XXX, XXX−XXX

this radical is a set of narrow resonance lines (indicated with filled circles in Figure 10) from another radical that decays above 100 K. Subtracting the EPR spectrum obtained at 200 K from the EPR spectrum obtained at 50 K gives the difference trace shown at the bottom, in which the lines of this radical are less obscured by other radicals present in the irradiated solid. This pattern corresponds to a doublet or triplet of quartets separated by ~20 G, which suggests that it is from an H adduct **9**, as shown in the inset (see Figure 16S, Supporting Information, for simulations). An examination of the EPR spectra shown in Figure 15S (Supporting Information) suggests that the resonance lines indicated by open circles in the 200 K trace in Figure 10 are also present at lower temperatures. We determined that in the progenitor of this radical, the unpaired electron is strongly coupled both to the ^{14}N nucleus and to all of the protons in the ring. By trial and error, we demonstrated that the only way to produce such a radical is through the loss of CO in radical **7d** (see the inset in Figure 10). In Figure 17S (Supporting Information), we refined our DFT estimates for hfcc's in this species to simulate the obtained EPR pattern. One of these parameter sets for radicals **7d** and **9** is given in Table 2. Due to the complexity of the EPR spectra, distortions from planarity in the radicals, and strong overlap of resonance lines from several spin centers, these parameters may require more refinement. However, it is clear that the acesulfamate anion undergoes fragmentation in the irradiated solid.

While EPR spectra of irradiated acesulfamate are different from those observed for other aromatic imides, the chemistry is similar: the anion undergoes reaction 11, forming (unstable) radical **2d** (that promptly decarbonylates to **7d**) and it traps an electron via reaction 12. This is followed by protonation and S−O bond dissociation, in either order, to form radical **8**. It also releases H atoms (reaction 17) that add to the double bond in the ring (reaction 19) to give radical **9**. Complications arise from low stability of the acesulfamate radicals rather than significant differences in the primary chemistry.

Figures 12 and 13 exhibit EPR spectra obtained from irradiated $P_{666,14}$ acesulfamate. In addition to the resonance lines from the C(−H)• radicals (cf. Figure 4), there are also lines of radical **8** (cf. Figures 10 and 11) indicated with arrows in Figure 12 and a quartet of narrow lines that can only be attributed to the $^{\bullet}CH_2-$ radical **10** shown in Figure 13 (the DFT estimates for hfcc constants are given in Table 2 and the caption to Figure 18S, Supporting Information). This radical can be generated via deprotonation of the oxidized anion from the methyl group or H abstraction from this group. Warming of the irradiated $P_{666,14}$ acesulfamate causes the transformation of its EPR spectra, as shown in Figure 13: radical anion **8** gradually decays, and the quartet of resonance lines from radical **10** becomes better resolved (see the simulation of the 100 K trace given in the plot). Above 150 K, the outer resonance lines of radical **10** exhibit additional structure. Such features can be reproduced by reducing the hfcc anisotropy and slightly increasing the difference between the nearly (magnetically) degenerate protons in this radical (Table 2 and Figure 18S, Supporting Information). Radical **10** appears to be the main product of acesulfamate oxidation in the ionic liquid.

Given that our EPR spectroscopy demonstrated poor radiation stability of acesulfamate, we did not pursue further studies of this anion.

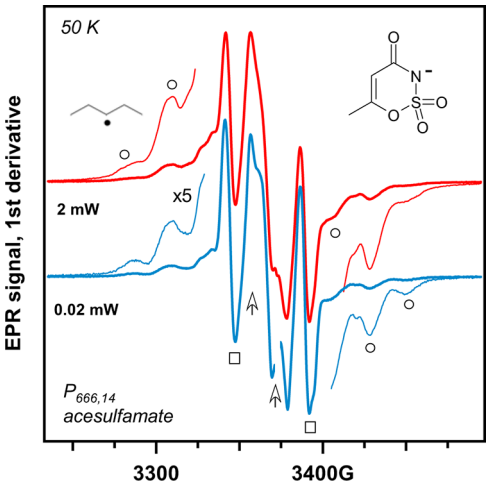

Figure 12. The EPR spectra of irradiated $P_{666,14}$ acesulfamate obtained at 50 K (for two microwave power levels). The resonance lines in the wings are from H loss radicals in the aliphatic arms of the cation (open circles); the two lines indicated by open squares are the outer lines of radical **10** shown at the bottom of Figure 13. The arrows indicate the resonance lines of radical **8** shown in Figure 11 that are superimposed on this quartet.

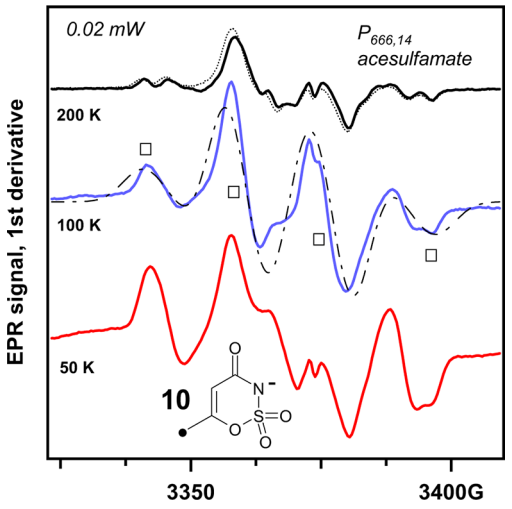

Figure 13. Temperature variation of the quartet from radical **10** (cf. Figure 12). The dotted trace is for the 200 K sample cooled back down to 50 K, and illustrates that these features are not due to motional effects. The dash-dot line is a simulated EPR spectrum for radical **10** shown in the inset (see also Table 2 and Table 2S and Figure 18S in the Supporting Information).

3.5. Mass Spectrometry and NMR. To complement our EPR studies, we analyzed irradiated liquid IL samples using NMR spectroscopy and ESI MS, as described in section 2.

Figures 19S and 20S (Supporting Information) exhibit the mass spectra for irradiated and nonirradiated $P_{666,14}$ saccharinate and *o*-benzenedisulfonimide, respectively. Prior to radiolysis, the largest mass peaks for these IL solutions correspond to the $C^+(CA)_n$ and $A^-(CA)_n$ ion species (n = 0, 1, and 2). During radiolysis, the $P_{666,14}^+$ cation fragments and the radical fragments disproportionate, recombine, and/or add to the imide anions, so the resulting mass spectra are quite complex. Importantly, neither one of the irradiated ILs indicates the occurrence of anion fragments with lower m/z than the parent anion, which suggests the relative stability of these imide anions. There are many weak mass peaks covering the region 20−100 amu to the right of the A^- peak (Figure 19S(a), Supporting Information), suggesting that alkyl radicals

dx.doi.org/10.1021/jp302151c | J. Phys. Chem. B XXXX, XXX, XXX−XXX

(fragments of the $P_{666,14}^+$ cation) add to the anion at the benzene ring (probably at the C_2 and C_3 carbons). Also observed are weak mass peaks (at ~0.1% ion counts of the main peaks) that are offset by $(M - 1)$ from these main mass peaks, where $M \approx 182$ amu is the mass of saccharinate (Figure 19S, Supporting Information). These peaks should be from a saccharinate dimer anion, which is generated when radical **2b** adds to the benzene ring of the parent saccharinate anion. The low yield of this dimer anion suggests that most of the imidyl radicals **2b** decay through H atom abstraction reaction 14 rather than this radical addition.

In the mass spectra of *o*-benzenedisulfonimide shown in Figure 20S(a) (Supporting Information), there are similar mass peaks (at 1% of the main peaks) that are offset by 155 amu (e.g., the m/z 373 peak). This mass offset corresponds to the loss of SO_2, so a possible explanation is that some radicals **2c** eliminate SO_2 and add to the parent anion at the benzene ring; alternatively, electronically excited anion **c** eliminates SO_2 and the resulting diradical adds to the parent anion. These reactions did not occur for saccharinate.

We emphasize that the yield of this SO_2 loss was small despite the very high radiation dose (which was ~5× higher than the highest projected dose accumulated over the lifetime of a diluent used for nuclear separations).[2,5] Another important consideration is that the dose *rate* in our experiments was >100× higher than in any practically relevant setting. As the yield of cross recombination strongly depends on the steady-state radical concentration, such reactions are less important in the low dose rate regime.

Figure 21S (Supporting Information) exhibits MS_2^- spectra obtained for m/z 218 (A^-), 373, and 919 (C_2A^-) peaks for $P_{666,14}$ *o*-benzenedisulfonimide, with each spectrum assigned a different color. In these experiments, the mass selected *o*-benzenedisulfonimide anions (±1 amu) are collisionally activated. The collision energy required to observe these anion fragmentations was ~3× higher than the energy required to fragment NTf_2^- to $TfN^{-\bullet}$ + $CF_3SO_2^\bullet$ and $TfNSO_2^{-\bullet}$ + $^\bullet CF_3$.[8] For the parent anion, the main fragmentation pathway is $C_6H_4S_2O_2^{-\bullet}$ + $NO_2^\bullet$. Note that no such fragmentation (nor other low-mass fragments) was observed in the MS_1^- spectra of the irradiated IL. The progenitor of the m/z 373 mass peak exhibits a complex fragmentation pattern, suggesting the elimination of $NO_2^\bullet$, SO_2, and $NHSO_2^\bullet$ fragments. This pattern is consistent with a dimer generated via a diradical ($^{-\bullet}NSO_2C_6H_5^\bullet$ that is formed by elimination of SO_2 from the electronically excited parent anion) adding to another *o*-benzenedisulfonimide anion; the resulting radical becomes the $NH_2SO_2C_6H_5{-}C_6H_3(SO_2)_2N^-$ anion. The CA_2^- anion (m/z 919) eliminates SO_2 or $H^{\delta+}A^{\delta-}$. We conclude that the mass spectra indicate good radiation stability of saccharinate (to ring-opening and contraction) but somewhat lower stability for *o*-benzenedisulfonimide, which can eliminate SO_2 from an excited state or some other reaction intermediate, albeit as a minor reaction.

Figure 22S (Supporting Information) exhibits the aromatic region of the ^{1}H NMR spectra from these two IL samples. As seen in this plot, the main contribution is from the parent imide anions; the resonance lines from other products are ~40× weaker. Taking the methyl protons of the $P_{666,14}^+$ cation as an internal standard, their aromatic protons as a group integrate to ≈4 H, but the parent anions integrate only to ≈3 H. The ^{1}H NMR spectra for these two ILs are quite similar, suggesting their common reactions. As the chemical shift for the ring protons would change significantly when the carbons in the benzene ring become substituted, these resonance lines belong to alkyl substituted parent anions generated by addition of radicals derived from the $P_{666,14}^+$ cation to the benzene ring of the parent anion. The same is suggested by the ^{13}C NMR spectra for aromatic carbons, as shown in Figures 23S and 24S (Supporting Information). While the NMR line intensities do not represent the abundances of the carbon-13 nuclei due to the differences in their spin−lattice relaxation time and short acquisition window (required to observe the low-yield products), the intact *o*-benzenedisulfonimide and saccharinate anions account for 90 and 85% of the aromatic-carbon signals, respectively. For *o*-benzenedisulfonimide, the resonance lines at 125.6 and 128.9 ppm account for 2.5% of the product yield (Figure 23S, Supporting Information); for saccharinate, a group of lines with chemical shifts between 125 and 128 ppm accounts for 4.5% of the product yield (Figure 24S, Supporting Information). For both of these anions, such resonance lines have a counterpart at ~138 ppm whose magnitude (relative to the 125−128 ppm lines) increases in the presence of a paramagnetic relaxant (that was added to shorten the longitudinal relaxation). We attribute these 125−128 ppm lines to unsubstituted carbon-13 in the substituted benzene ring, and the ~138 ppm lines to the substituted carbon in this ring. In addition to these NMR lines, there are many unattributed lines with <1% relative yield.

These NMR results indicate that the aromatic imide anions are quite robust, and the extent of decomposition/modification of the *o*-benzenedisulfonimide anion is not considerably greater than that of the saccharinate anion, even under high dose rate conditions.

4. DISCUSSION

Our results indicate the remarkable radiation stability of aromatic imide anions **a**−**c** shown in Scheme 1 but lower stability of acesulfamate (anion **d**). The stability of these aromatic imides is even more noteworthy given that their N-alkyl derivatives are photochemically active:[31] the triplet state readily abstracts an H atom from the alkyl arm (or the solvent), forming a biradical (or a radical pair) involving the ketyl radical **6** shown in Scheme 2. These ketyl radicals are isomers of radicals **1** and **3**. Our DFT calculations indicate that radical **6** is always less stable than radical **1** (by 0.26 for X = SO_2 and 0.79 eV for X = CO) because the $>N^-$ moiety is a stronger base than the carbonyl group, so the proton preferably binds to the nitrogen site. This conclusion is supported by the studies of ref 8, as the observed radical chemistry for the phthalimide anion is consistent with a one-electron transfer reaction 16 rather than the formation of radical **6** as an intermediate. The formation of the latter radical is also inconsistent with the observed EPR spectra (see Table 2S, Supporting Information, for predicted hyperfine coupling constants).

Table 1 summarizes the energetics of the examined anions. The proton affinity of these anions correlates well with their pK_a's in aqueous solutions (section 1), and gas-phase electron detachment energies cluster around 4.0−4.4 eV, which is significantly lower than this energy for NTf_2^- (~5.5 eV), so the corresponding radicals are weaker oxidizers. This is beneficial for radioprotection of the solute, as the resulting radical **2** is more likely to decay in reaction 14 than to oxidize the solute.

The adiabatic electron affinity of these imides is considerable (~1 eV), which accounts for the ease of their reduction. The triplet states of these anions are quite low in energy (our DFT

dx.doi.org/10.1021/jp302151c | J. Phys. Chem. B XXXX, XXX, XXX−XXX

calculation gives 2.9−3.1 eV vs the experimental estimate of 3.5 eV for phthalimide).[23] Our calculations also suggest that the N−C_O and N−S bond scission in the lowest triplet state are strongly exergonic for all anions with the exception of *o*-benzenedisulfonimide.

Radicals **1**, **3**, and **6** can all be formally regarded as H atom adducts of the parent anion. In all cases but one, the electronic energy of radical **1** is lower than that of radical **3** or **6**. The observed formation of radical **3**, therefore, suggests two competing pathways for reduction: radical **1** is generated via reactions 12 and 13, whereas radical **3** is generated in reactions 17 and 19. The exception is *o*-benzenedisulfonimide, for which the ring addition that yields radical **3c** is more exergonic than radical **1c** formation (Table 1). For aromatic imides, radical **1** is very stable, as the excess electron is shared by the π-orbital of the benzene ring, while for acesulfamate this radical anion is unstable and fragments to radical **8** (Scheme 2S, Supporting Information). The most exergonic reaction of this radical anion involves ring-opening at the weakened S−O bond. The simulated EPR spectrum of the lowest energy open-ring structure (radical **8**) provides a good fit to the EPR spectrum shown in Figure 11, whereas no other structure in Scheme 2S (Supporting Information) yields this EPR spectrum. We suggest that ring-opening in radical **1d** occurs even at 77 K due to the weakness of the S−O bond in this radical (see Scheme 2S, Supporting Information, for energetics).

We turn to radical **2**, whose stability was the original concern of this study. As mentioned in the Introduction, we expected that some stabilization of this imidyl radical could occur via reaction 15. The estimates given in Table 1 indicate that the N−N bonding energy in the gas phase, C_2 symmetrical dimer anion **4** rapidly decreases from 0.79 to 0.35 eV as the carbonyl groups are replaced with sulfonyl groups that introduce steric hindrance (see Figure 3S, panel b, Supporting Information). Given this weak interaction, it seems unlikely that such stabilization is important.

As seen from Table 1 and the energy diagrams given in Figures 25S−27S (Supporting Information), the imidyl radical is quite stable toward the dissociation of C_r−C_O and C_r−S bonds involving the ring carbons, but it is much less stable to elimination of CO and, especially, SO_2. For radical **2d** (Figure 27S, Supporting Information), both of these elimination reactions are exergonic, and the decarbonylated radical **7d** has the lowest energy. This accords with the results of section 3.4, suggesting the presence of such a radical in irradiated potassium acesulfamate. For radical **2b** (Figure 25S, Supporting Information), these reactions are nearly thermoneutral, yet no *o*-substituted phenyl radicals were observed, suggesting that this fragmentation involves a high reaction barrier. Our DFT calculations (see Figures 25S and 26S, Supporting Information) also indicate that elimination of SO_2 from radicals **2b** and **2c**, which results in contraction of the ring, is exergonic. Unlike radical **2**, the resulting radical **7** (which has a hfcc tensor for ^{14}N similar to radical **2**) is predicted to have non-negligible hfcc's on the ring protons (Table 2S, Supporting Information), which would result in a different EPR spectrum from the one observed experimentally (cf. Figure 9S(b), Supporting Information). Thus, our EPR observations indicate the stability of imidyl radicals in the crystalline matrix.

The likely cause for this stability is that the elimination of SO_2 and CO requires sequential cleavage of two bonds that involve high reaction barriers (see Figures 25S and 26S, Supporting Information). The same applies to the parent anions: while elimination of SO_2 (Scheme 3S, reaction a, Supporting Information) is energetically favorable for triplet anions, the intermediate triplet diradical anion is >1 eV higher in energy than this triplet state, so the elimination of SO_2 can only involve the excited singlet or higher triplet states. As we have seen in section 3.5, even collisional activation of anion **c** does not result in SO_2 elimination but rather causes $NO_2^{\bullet}$ elimination which is a less exergonic reaction in the gas phase (Figure 26S, Supporting Information).

Radical **2** can serve not only as an electron acceptor but also as an H atom acceptor (reaction 14 is an example of such reactivity). The experimental estimate of the N−H bond energy for anion **a** in tetramethylene sulfone is 3.86 eV;[31] for the gas-phase molecule, our DFT calculation gives a much higher bond energy of 5.4 eV; for anions **b** and **c**, this energy is 10 and 20% lower, respectively. This high N−H bond energy rationalizes previous observations[22,23] that, in acetonitrile solutions, radical **2** abstracts an H atom from toluene, anisole, triethylamine, ethers, and *N*,*N*′-dimethylaniline, for which the gas-phase C−H bond dissociation energies are ∼4 eV. Reaction 14 may account for the difficulty of observing radical **2** in the corresponding ILs (as opposed to the corresponding alkali salts, see section 3.1). It also rationalizes the low yield of the dimeric anion generated when radical **2b** adds to the benzene ring in the parent anion (section 3.5).

Radical **1a** is known to react with other radicals that attach to the carbonyl carbon (Scheme 1S, Supporting Information).[22,23] This addition can also occur for radical **1b**; however, such reactions are impossible for radical **1c**, so it is likely to decay by back electron or proton transfer, e.g.,

$$>NH^{-\bullet} + C(-H)^{\bullet} \rightarrow >N^{-} + C^{+} \qquad (20)$$

As observed in the Introduction, the redox stability of IL anions is a necessary but not sufficient condition for radiation stability of the IL, as the excited states of these anions should also be stable. Our DFT calculations suggest that the most favorable dissociation channel possible for triplet excited states of anions **b** and **c** (Figures 25S and 26S (Supporting Information), respectively) is S−N bond dissociation with the formation of a diradical anion that is similar to reaction 10b. The resulting diradical can further undergo SO_2 loss. There is a report in the literature,[32] suggesting the occurrence of such SO_2 loss and the subsequent termination of the diradical for N-alkyl saccharin photolyzed in alcohol and benzene (Scheme 3S, reaction a, Supporting Information). A photoisomerization for saccharin-related sultams and their N-alkyl and N-aryl derivatives that involves the transfer of the oxygen from sulfur to nitrogen, as shown in Scheme 3S, reaction b, in the Supporting Information has also been reported.[32] In the gas phase, this rearrangement (for saccharin, >NH) is endoergic by 1.23 eV, so it can proceed from an excited state; however, our DFT calculations indicate that the corresponding species for the parent anion ($>N^-$) is not bound, so this isomerization channel is very unlikely. Given the occurrence of SO_2 loss, giving the dimer anion in the mass spectra of irradiated $P_{666,14}$ *o*-benzenedisulfonimide (but not $P_{666,14}$ saccharinate, see section 3.5), it seems that a reaction analogous to that shown in Scheme 3S(a) (Supporting Information) may occur in the former IL.

While such fragmentation reactions for electronically excited anions do seem to occur as a minor channel (section 3.5), it seems likely (given the availability of reducible anions in the ILs) that the corresponding excited states mainly decay via

dx.doi.org/10.1021/jp302151c | J. Phys. Chem. B XXXX, XXX, XXX−XXX

reaction 16 and/or excited-state quenching without yielding fragments. For saccharinate, there is no experimental evidence for SO_2 elimination, while, for *o*-benzenedisulfonimide, the radiolytic yield for the SO_2 loss seems to be less than ~0.05 anions per 100 eV, which is tolerably low for most applications.

5. CONCLUDING REMARKS

What anions can be used to constitute practically useful ILs exhibiting maximal stability upon exposure to ionizing radiation?

Our previous research indicated that, unfortunately, the majority of the anions currently used for IL synthesis are unstable to varying degrees upon irradiation, as fragmentation occurs from various oxidized, reduced, or electronically excited states. Furthermore, the failure of IL diluents to protect radiation damage to certain extracting agents (such as crown ether ionophores[10] and diglycolamides[11]) is caused by transfer of oxidation and/or excitation to the solute: the anions that do not fragment (which tend to have high electron detachment energies) serve as efficient oxidizers, whereas the anions that have low electron detachment energies tend to fragment. We have consequently used our findings to seek anions that exhibit (i) relatively low electron detachment energy and (ii) high stability to fragmentation in their electronically excited, reduced, and oxidized states.

We argue that aromatic imides shown in Scheme 1, whose properties occupy a "sweet spot" of radiation stability, could be such optimum IL anions. Our EPR studies indicate that oxidized and reduced forms of these anions are stable and their reactions (such as H atom addition) do not result in fragmentation. With the exception of acesulfamate, we found no evidence for extensive bond breaking and small-fragment elimination from the corresponding radicals and excited states. The ultimate cause for this stability of the aromatic imide anions in *ionic* liquids is similar to that for aromatic molecules in *molecular* liquids: the existence of extended π-orbitals that can spread the extra charge or excitation over their entire structure, minimizing the weakening of individual bonds.

While all three aromatic imides shown in Scheme 1 exhibit this exceptional radiation stability, *o*-benzenedisulfonimide presents the greatest interest for nuclear separations, because this anion is not protonated when the corresponding IL contacts acidic solutions. This protonation enables undesirable transformation of the IL diluent into a mixture of salts.[14] Furthermore, phthalimide-based ILs are suitable for extractions from basic solutions, and saccharinate-based ILs are suitable for weakly acidic solutions. Thus, there is an optimal solution for each proticity range. Saccharinate-based ILs have already attracted much attention as "greener" solvents (due to their low toxicity).[26−28] Remarkably, these greener ILs also appear to be most suitable for applications in high radiation fields.

■ ASSOCIATED CONTENT

Supporting Information

A PDF file containing a list of abbreviations and reactions, synthetic procedures (section 1S), crystallographic parameters (section 2S), Tables 1S and 2S, and Figures 1S−27S with captions, including the experimental and simulated EPR spectra. This material is available free of charge via the Internet at http://pubs.acs.org.

■ AUTHOR INFORMATION

Corresponding Author

*Phone: (630) 252-9516. E-mail: shkrob@anl.gov.

Notes

The authors declare no competing financial interest.

■ ACKNOWLEDGMENTS

We thank R. Lowers, D. Quigley, J. Schlueter, and J. Muntean for technical support. The work at Argonne and Brookhaven was supported by the US-DOE Office of Science, Division of Chemical Sciences, Geosciences and Biosciences under Contracts Nos. DE-AC02-06CH11357 and DE-AC02-98CH10886, respectively. Programmatic support via a DOE SISGR grant "An Integrated Basic Research Program for Advanced Nuclear Energy Separations Systems Based on Ionic Liquids" is gratefully acknowledged.

■ REFERENCES

(1) Hallett, J. P.; Welton, T. *Chem. Rev.* **2011**, *111*, 3508−3576. Welton, T. *Chem. Rev.* **1999**, *99*, 2071−2084. Plechkova, N. V.; Seddon, K. R. *Chem. Soc. Rev.* **2008**, *37*, 123−150. Metlen, M. S. A.; Rogers, R. D. *Acc. Chem. Res.* **2007**, *40*, 1182−1192. Parvulescu, V. I.; Hardacre, C. *Chem. Rev.* **2007**, *107*, 2615−2665. Binnemans, K. *Chem. Rev.* **2007**, *107*, 2592−2614.

(2) Sun, X.; Luo, H.; Dai, S. *Chem. Rev.* **2012**, *112*, 2100−2128.

(3) Billard, I.; Ouadi, A.; Gaillard, C. *Anal. Bional. Chem.* **2011**, *400*, 1555−1566.

(4) Ha, S. H.; Menchavez, R. N.; Koo, Y.-M. *Korean J. Chem. Eng.* **2010**, *27*, 1360−1365.

(5) Wishart, J. F. *J. Phys. Chem. Lett.* **2010**, *1*, 3225−3231. Wishart, J. F.; Shkrob, I. A. In *Ionic Liquids: From Knowledge to Application*; Rogers, R. D., Plechkova, N. V., Seddon, K. R., Eds.; American Chemical Society: Washington, DC, 2009; pp 119−134.

(6) Berthon, L.; Chabronnel, M.-C. In *Ion Exchange and Solvent Extraction, A Series of Advances*, Vol. *19*; Moyer, B. A., Ed.; CRC Press: Boca Raton, FL, 2010; pp 429−513.

(7) Shkrob, I. A.; Chemerisov, S. D.; Wishart, J. F. *J. Phys. Chem. B* **2007**, *111*, 11786−11793.

(8) Shkrob, I. A.; Marin, T. W.; Chemerisov, S. D.; Wishart, J. F. *J. Phys. Chem. B* **2011**, *115*, 3872−3888.

(9) Shkrob, I. A.; Marin, T. W.; Chemerisov, S. D.; Hatcher, J. L.; Wishart, J. F. *J. Phys. Chem. B* **2011**, *115*, 3889−3902.

(10) Shkrob, I. A.; Marin, T. W.; Dietz, M. L. *J. Phys. Chem. B* **2011**, *115*, 3903−3911.

(11) Shkrob, I. A.; Marin, T. W.; Bell, J. R.; Luo, H.; Dai, S.; Hatcher, J. L.; Rimmer, R. D.; Wishart, J. F. *J. Phys. Chem. B* **2011**, *116*, 2234−2243.

(12) Shkrob, I. A.; Wishart, J. F. *J. Phys. Chem. B* **2009**, *113*, 5582−5592.

(13) Korth, H. G.; Chateauneuf, J.; Lusztyk, J.; Ingold, K. U. *J. Org. Chem.* **1991**, *56*, 2405−2410 and references therein.

(14) Marin, T. W.; Shkrob, I. A.; Dietz, M. L. *J. Phys. Chem. B* **2011**, *115*, 3912−3918.

(15) (a) Huang, W.; Chen, S.; Liu, Y.; Fu, H.; Wu, G. *Radiat. Phys. Chem.* **2011**, *80*, 573−577. (b) Huang, W.; Chen, S.; Liu, Y.; Fu, H.; Wu, G. *Radiat. Phys. Chem.* **2011**, *80*, 573−577. (c) Yuan, L.; Peng, J.; Zhai, M.; Li, J.; Wei, G. *Radiat. Phys. Chem.* **2009**, *78*, 737−739. (d) Qi, M.; Wu, G.; Chen, S.; Li, Y. *Radiat. Res.* **2007**, *167*, 508−514.

(16) Berthon, L.; Nikitenko, S. I.; Bisel, I.; Berthon, C.; Faucon, M.; Saucerotte, B.; Zorza, N.; Moisy, Ph. *Dalton Trans.* **2006**, 2526−2534. Le Rouzo, G.; Lamouroux, C.; Dauvois, V.; Dannoux, A.; Legand, S.; Durand, D.; Moisy, P.; Moutiers, G. *Dalton Trans.* **2009**, 6175−6184. Allen, D.; Baston, G.; Bradley, A. E.; Gorman, T.; Haile, A.; Hamblett, I.; Hatter, J. E.; Healey, M. J. F.; Hodgson, B.; Lewin, R.; Lovell, K. V.; Newton, B.; Pitner, W. R.; Rooney, D. W.; Sanders, D; Seddon, K. R.; Sims, H. E.; Thied, R. C. *Green Chem.* **2002**, *4*, 152−158.

(17) Yuan, L.; Xu, C.; Peng, J.; Xu, L.; Zhai, M.; Li, J.; Wei, G.; Shen, X. *Dalton Trans.* **2009**, 7873−7875. Yuan, L. Y.; Peng, J.; Xu, L.; Zhai, M. L.; Li, J. Q.; Wei, G. S. *J. Phys. Chem. B* **2009**, *113*, 8948−8952. Yuan, L. Y.; Peng, J.; Xu, L.; Zhai, M. L.; Li, J. Q.; Wei, G. S. *Dalton Trans.* **2008**, 6358−6360.
(18) Kasai, P. H. *J. Am. Chem. Soc.* **1992**, *114*, 2875−2880. Lind, J.; Jonsson, M.; Eriksen, T. E.; Merenyi, G.; Eberson, L. *J. Phys. Chem.* **1993**, *97*, 1610−1614.
(19) Nelsen, S. F. *J. Am. Chem. Soc.* **1967**, *89*, 5256−5259.
(20) For example: Sugo, Y.; Izumi, Y.; Yoshida, Y.; Nishijima, S.; Sasaki, Y.; Kimura, T.; Sekine, T.; Kudo, H. *Radiat. Phys. Chem.* **2007**, *76*, 794−800.
(21) See the following for a general introduction to photochemistry of phthalimide and its derivatives: Griesbeck, A. G.; Hoffmann, N.; Warzecha, K.-D. *Acc. Chem. Res.* **2007**, *40*, 128−140.
(22) Sanchez-Sanchez, C.; Perez-Inestrosa, E.; Garcia-Segura, R.; Suau, R. *Tetrahedron* **2002**, *58*, 7267−7274.
(23) Horvat, M.; Mlinaric-Majerski, K.; Basaric, N. *Croatica Chem. Acta* **2010**, *83*, 179−188.
(24) Blaschette, A.; Jones, P. G.; Hamann, T.; Näveke, M.; Schomburg, D.; Cammenga, H. K.; Epple, M.; Steppuhn, I. *Z. Anorg. Allg. Chem.* **1993**, *619*, 912−922.
(25) Hendrickson, J. B.; Okano, S.; Bloom, R. K. *J. Org. Chem.* **1969**, *34*, 3434−3438.
(26) Nockemann, P.; Thijs, B.; Driesen, K.; Janssen, C. R.; Van Hecke, K.; Van Meervelt, L.; Kossmann, S.; Kirchner, B.; Binnemans, K. *J. Phys. Chem. B* **2007**, *111*, 5254−5263.
(27) Pernak, J.; Stefaniak, F.; Węglewski, J. *Eur. J. Org. Chem.* **2005**, 650−652. Stasiewicz, M.; Mulkiewicz, E.; Tomczak-Wandzel, R.; Kumirska, J.; Siedlecka, E. M.; Golebiowski, M.; Gajdus, J.; Czerwicka, M.; Stepnowski, P. *Ecotoxicol. Environ. Saf.* **2008**, *71*, 157−165.
(28) Carter, E. B.; Culver, S. L.; Fox, P. A.; Goode, R. D.; Ntai, I.; Tickell, M. D.; Traylor, R. K.; Hoffman, N. W.; Davis, J. H., Jr. *Chem. Commun.* **2004**, 630−631.
(29) Becke, A. D. *Phys. Rev. A* **1988**, *38*, 3098. Lee, C.; Yang, W.; Parr, R. G. *Phys. Rev. B* **1988**, *37*, 785.
(30) Frisch, M. J.; Trucks, G. W.; Schlegel, H. B.; Scuseria, G. E.; Robb, M. A.; Cheeseman, J. R.; Zakrzewski, V. G.; Montgomery, J. A., Jr.; Stratmann, R. E.; Burant, J. C.; et al. *Gaussian 98*, rev. A.1; Gaussian, Inc.: Pittsburgh, PA, 1998.
(31) Arnett, E. M.; Venimadhavan, S.; Amaranath, K. *J. Am. Chem. Soc.* **1992**, *114*, 5598−5602.
(32) Döpp, D. *Int. J. Photoenergy* **2001**, *3*, 41−47.